Computed Tomography of the Liver

Domenico De Santis, Federica Landolfi, Marta Zerunian, Damiano Caruso, and Andrea Laghi

Contents

1 **Introduction** ... 78

2 **Patient Preparation** ... 78
2.1 Renal Adverse Reactions ... 78

3 **Contrast Media Administration** ... 79

4 **MDCT: Technical Parameters** ... 80

5 **Multiphasic Approach** ... 81
5.1 Unenhanced Phase ... 81
5.2 Contrast-Enhanced Phases ... 81

6 **CT Perfusion** ... 82

7 **Image Reconstruction** ... 86
7.1 Filtered Back Projection ... 86
7.2 Iterative Reconstruction ... 87

8 **Post-processing Techniques** ... 87
8.1 Multiplanar Reformatting (MPR) ... 88
8.2 Maximum Intensity Projection (MIP) ... 89
8.3 Minimum Intensity Projection (MinIP) ... 89
8.4 Volume Rendering (VR) ... 90

9 **Dual-Energy CT: Basic Principles and Technical Parameters** ... 91

10 **Dual-Energy CT: Post-processing** ... 92
10.1 Blended Images ... 92
10.2 Basis Material Decomposition ... 92
10.3 Iodine Maps ... 93
10.4 Virtual Non-contrast Images ... 94
10.5 Virtual Monoenergetic Images ... 94

D. De Santis · F. Landolfi · M. Zerunian · D. Caruso
A. Laghi (✉)
Department of Surgical and Medical Sciences and Translational Medicine, School of Medicine and Psychology, "Sapienza"—University of Rome, Sant'Andrea University Hospital, Rome, Italy
e-mail: andrea.laghi@uniroma1.it

© Springer Nature Switzerland AG 2021

E. Quaia (ed.), *Imaging of the Liver and Intra-hepatic Biliary Tract*,
Medical Radiology, Diagnostic Imaging, https://doi.org/10.1007/978-3-030-38983-3_4

11 Future Perspective: Photon-Counting CT 95
References 96

Abstract

Multidetector Computed Tomography (CT) plays a pivotal role in the evaluation of liver pathologies due to its fast acquisition time, thinner image thickness and narrow collimation, resulting in high temporal and spatial resolution, fundamental to detect subtle liver lesions and to optimize radiation exposure.

State-of-the-art liver imaging requires proper patient preparation, the implementation of optimized contrast dye injection strategies, and a thorough CT scanner configuration.

A multiphasic CT examination is mandatory to maximize diagnostic performances in terms of lesion identification and is the current choice in daily clinical practice. In the other hand, functional imaging, such as CT perfusion, provides quantitative parameters that improve diagnostic capabilities in selected cases. Operators needs to know different imaging reconstruction strategies and master all the available post-processing techniques, in order to select the best option in every clinical scenario. Over the last decades, Dualenergy CT has further expanded the diagnostic possibilities in liver imaging and is currently widely implemented in multiple Institutions worldwide. Eventually, photon-counting CT is the very latest technical advancement in CT imaging and is at the forefront of scientific research, bearing the potential to revolutionize liver imaging.

1 Introduction

Multiphasic computed tomography (CT) is one of the leading imaging techniques in the evaluation of liver diseases. Since its introduction in the 1970s, multiple technical improvements have expanded its clinical capabilities to the point that CT currently plays a pivotal role in the diagnosis and management of liver diseases, both in emergency and in elective clinical scenarios. This chapter provides a technical overview on multiphasic liver CT, including patient preparation, contrast media administration techniques, CT technical parameters, current technology, and future perspectives.

2 Patient Preparation

No specific patient preparation is recommended, but fasting for at least 6 h prior to the examination in case of intravenous contrast medium (CM) administration is required.

Positive oral CM is not deemed necessary for abdominopelvic CT scan: neutral contrast agent, as water, may be used as equally effective with a dose of 500–600 mL (Lee et al. 2013, 2016).

As general recommendation to a CT scan, it is advisable to remove any clothes and, if possible, any metallic item which can produce artifacts, reducing diagnostic performance of the examination (Barrett and Keat 2004).

A proper peripheral intravenous access must be placed to ensure high-quality angiographic and parenchymal studies. Choosing the most appropriate vascular access allows to avoid complications such as extravasation of CM: the preferred route is the antecubital or forearm area. However, central lines such as peripherally inserted central catheters or port-a-cath devices might be used, as long as long they are marked as "power injectable," not exceeding the maximum flow rate printed on the catheter itself (Williamson and McKinney 2001).

Patients who undergo CT scan with intravenous administration of iodinated CM must be screened to estimate the risk of renal and nonrenal adverse reactions.

2.1 Renal Adverse Reactions

Renal adverse effects consist of renal function deterioration in a short time window after intravascular administration of iodinated CM (van der

Molen et al. 2018a). Until a few years ago any decrease in renal function occurring after CM administration used to be considered as contrast-induced nephropathy in the absence of an alternative etiology. However, a high rate of fluctuation in kidney function occurs even in patients without exposure to iodinated CM (Bruce et al. 2009), making it challenging to determine whether or not CM is the actual determinant of renal function deterioration. Postcontrast acute kidney injury (PC-AKI) is defined as an increase in serum creatinine (sCr) ≥0.3 mg/dL (or ≥26.5 μmol/L), or sCr ≥1.5–1.9 times baseline, within 48–72 h of intravascular administration of CM (Thomas et al. 2015; Ad-Hoc Working Group of E et al. 2012). The most important risk factors for PC-AKI are impaired renal function (eGFR less than 30 mL/min/1.73 m^2 before CM intravenous administration), dehydration, and repeated CM administration within a short interval (48–72 h) (van der Molen et al. 2018a). Other possible predisposing factors may be identified in old age, female gender, low BMI, cardiovascular diseases, and metabolic factors (Moos et al. 2013; Kanbay et al. 2017; Kwasa et al. 2014).

Patient's serum creatinine level is necessary to derive the estimated glomerular filtration rate (eGFR) by applying the modification of diet in renal disease (MDRD) equation or the chronic kidney disease epidemiology collaboration (CKD-EPI) equation. The latter formula is recommended since it allows a more accurate categorization of patients at lower risk of chronic kidney disease into higher eGFR categories (van der Molen et al. 2018a). Each patient eGFR should be estimated before the CT examination in order to safely inject CM.

Details about PC-AKI and its medical management go beyond the purpose of this chapter. However, it is worth to mention that oral hydration alone does not prevent PC-AKI and that modern nonionic iodinated CM can also be safely administered to patients with hematologic disorders with normal renal function (van der Molen et al. 2018b). As a general rule, the incidence of PC-AKI is related to the dose of CM and therefore it is recommended to use the lowest dose of contrast medium to obtain a diagnostic examination (Stacul et al. 2011).

3 Contrast Media Administration

The CM intensifies the attenuation differences between healthy liver parenchyma and focal liver lesions, improving lesions' conspicuity and detectability. A multiphasic approach is mandatory to correctly identify and characterize focal liver lesions.

Liver contrast enhancement (CE) results from distribution of CM into the extravascular interstitial space and is related to *iodine concentration* and *iodine delivery rate* (IDR—mg of iodine entering the circulation per second, which depends on flow rate) and amount of injected CM. The quality of liver enhancement during the arterial phase is strictly dependent on the injection rate, while parenchymal enhancement during portal venous phase and delayed phase is determined by the total dose of iodine administered and is less dependent on the injection rate, due to CM recirculation phenomenon (Bae 2010). The optimal flow rate for a proper CE of liver parenchyma should be 3–4 mL/s or higher, allowing for an optimal temporal separation between pure arterial and portal venous phase. Injection rates of 5–10 mL/s are generally reserved to CT perfusion studies (Laghi 2007).

Highly concentrated CM (350, 370, and 400 mgL/mL) allows to reach adequate IDRs even when a low flow rate is mandatory due to small-caliber i.v. access. When highly concentrated CM, even if in a small volume, is administered at a fixed injection rate, a fast delivery of iodine mass per unit time occurs, resulting in an earlier and greater arterial peak enhancement even if shorter in duration: the magnitude of overall hepatic enhancement is not substantially affected during venous and delayed phases, but the detection of hypervascular lesions is improved (Awai et al. 2002).

A parenchymal enhancement of 50 HU is required for diagnostic purposes and it has been demonstrated that the iodine load required to reach such enhancement is slightly higher than 500 mgL/kg (Heiken et al. 1995). Therefore, patient's size plays a fundamental role in contrast enhancement and has to be considered when performing a contrast-enhanced CT scan. Although

total body weight is the most widely used parameter in clinical practice, it must be considered that body fat contributes minimally in dispersing CM. Therefore, the risk of adjusting the amount of iodine load for the body weight, using a 1:1 linear scale, is an overestimation of the required amount of CM in obese patients. It has been established that lean body weight (LBW) is a more accurate method to estimate the iodine dose required to obtain a congruous liver enhancement (Kondo et al. 2010). LBW can be estimated by Boer formula (Boer 1984):

$$\mathrm{LBW}_{\mathrm{male}}^{\mathrm{Boer}} = (0.407 \bullet W) + (0.267 \bullet H) - 19.2$$

$$\mathrm{LBW}_{\mathrm{female}}^{\mathrm{Boer}} = (0.252 \bullet W) + (0.473 \bullet H) - 48.3$$

where W represents the patient weight in kilograms and H the patient height in meters, or by James formula (James et al. 1976), as follows:

$$\mathrm{LBW}_{\mathrm{male}}^{\mathrm{James}} = (1.10 \bullet W) - 128 \bullet \left[\frac{W^2}{(100 \bullet H)^2} \right]$$

$$\mathrm{LBW}_{\mathrm{female}}^{\mathrm{James}} = (1.07 \bullet W) - 148 \bullet \left[\frac{W^2}{(100 \bullet H)^2} \right]$$

where W represents the patient weight in kilograms and H the patient height in meters.

While both formulas provide equal results in the vast majority of patients, Boer formula better estimates the LBW in obese patients, and therefore it is one of the first choices in such subpopulation (Caruso et al. 2018).

Additional patient-related parameters affecting contrast enhancement include cardiac output, age, gender, venous access, and some pathologic hepatic conditions such as hepatomegaly and/or diffuse parenchymal diseases such as cirrhosis, which may be associated with decreased hepatic enhancement because of reduced portal venous perfusion related to fibrosis and increased hepatic resistance (Bae 2010).

A saline chaser (up to 50 mL) should follow the CM injection to improve bolus geometry and avoid the waste of a certain volume of CM that, otherwise, would remain in "dead spaces" such as the injector tubing, the peripheral veins, the right heart, or the pulmonary circulation. The bolus chaser also increases hydration and washes out any residual CM which may obstruct the i.v. access, especially in case of central venous access.

Scanning the liver at predetermined time points and employing fixed scan delay without taking into account specific patient and/or CM characteristics should be avoided (Laghi 2007). It is strongly preferable to employ precise methods to monitor CM arrival time and accurately calculate the scan delay, such as test bolus and bolus tracking:

- *Test bolus* consists of injecting a small bolus (10–20 mL) of CM before injecting the full amount of CM, after placing a region of interest (ROI) in a target district, generally at the starting level of the diagnostic sca. Sequential monitoring images are acquired, obtaining a time-enhancement curve of contrast enhancement within the ROI. The interval time needed to determine the peak of contrast enhancement is used to estimate scan delays for full-bolus diagnostic CT.
- *Bolus tracking* method consists of the injection of full diagnostic bolus of CM, administered without performing any prior test, while scanning a single level in upper abdomen with a ROI placed in aorta, generally at the level of celiac axis during a pre-contrast acquisition. Low-radiation-dose sequential images are acquired every 1–3 s providing a time-attenuation curve which maps the arrival time of contrast material; when a predetermined threshold (generally around 150–180 HU) has been reached, the diagnostic scan is triggered. An additional delay, called diagnostic delay, corresponding to the interval time running from the trigger to scan initiation, must be added.

4 MDCT: Technical Parameters

Since its advent, multi-detector CT represented a dramatic technical advance over single-detector scanners. Its rapid volume coverage speed and faster acquisition time, combined with thinner image thickness and narrow collimation, result in time-efficient image acquisition of large body

volumes and, therefore, in high temporal and spatial resolution.

Thin sections minimize partial-volume artifacts but also increase image noise and decrease length of coverage (Hu et al. 2000). A reduced coverage can be counteracted by increasing the pitch, defined as the ratio between the distance of the CT table per 360° gantry rotation and the X-ray beam collimation width. A pitch ≤1 is generally considered adequate in liver imaging (Laghi 2007).

Tube potential (kVp) and tube current (mAs) are the two main parameters affecting radiation exposure. A kVp reduction improves tissue contrast, but also increases image noise: in standard liver imaging a tube potential of 120 kVp is usually preferred, reserving 140 kVp for obese patients.

Automated tube voltage and tube current modulation systems have been introduced with the aim to optimize the radiation exposure. Depending on the attenuation differences of the various anatomic regions obtained during the scout scan, such systems automatically module kVp and mAs throughout the diagnostic scan to achieve a predefined level of image noise, reducing radiation exposure (Spearman et al. 2016).

5 Multiphasic Approach

Liver parenchyma ought to be studied before and after i.v. CM administration, by adopting proper delayed scan times in order to obtain arterial phase, portal-venous phase, and delayed phase, chosen on a case-by-case basis, aiming at tailoring the scan protocol to each patient and clinical scenario.

5.1 Unenhanced Phase

Although its utility is sometimes debated, the unenhanced phase still plays an important role in liver imaging. In fact, in several clinical scenarios, it proves to be a very helpful tool in the characterization of focal lesions such as focal hemorrhage, fat, or calcifications, which are easily recognized before contrast enhancement (Casillas et al. 2000; Patnana et al. 2018; Pickhardt et al. 2012). Additionally, an unenhanced phase should be performed in the evaluation of every cirrhotic liver and during follow-up of oncologic patients, in which non-contrast images may reveal a useful tool to differentiate benign from malignant focal liver lesions (Federle and Blachar 2001). CT scans acquired prior to CM injection are also extremely important in monitoring patients who underwent hepatic chemoembolization, demonstrating in detail the distribution of chemoembolization material (Johnson and Fishman 2013).

5.2 Contrast-Enhanced Phases

Liver has a unique dual circulatory dynamic: approximately 75–80% of the hepatic blood flow is supplied by the portal venous system, whereas the remaining 20–25% comes from the hepatic artery. Inherent consequences reflect in both normal and pathologic vasculature of liver parenchyma and focal lesions, respectively.

Hepatic arterial phase (AP) depicts liver parenchyma at the time CM reaches the aorta and the hepatic arteries, before it circulates through the spleen and the mesentery opacifying the portal venous system, generally 30–40 s later (Federle and Blachar 2001).

In a proper AP liver parenchyma is minimally enhanced and hepatic arteries display a conspicuous opacification. No enhancement of the hepatic veins should be obtained, whereas just some enhancement of the portal vein should be accomplished. AP can be subdivided into an *early arterial phase (EAP)* and a *late arterial phase (LAP)*, during which the hepatic enhancement predominantly reflects the arterial inflow through the hepatic arteries and an initial, thus relatively minor, tranche of splanchnic venous inflow through the portal vein (Foley 2002).

EAP starts approximately 25 s after initiating contrast injection, and lasts approximately 8–10 s. Therefore, to obtain a proper EAP by means of bolus tracking technique, a diagnostic delay ≤6 s should be selected (Laghi 2007; Foley 2002). Acquiring such phase should be reserved

to cases in which CT angiography would be of proven benefit by providing a tool for therapy planning. The most frequent indications to perform an EAP are:

- Defining arterial anatomy and anomalies, such as arterial stenosis, aberrant or replaced hepatic arteries
- Preoperative imaging in patients who are candidates for surgical hepatic resection and/or percutaneous ablation therapy

LAP occurs 35–45 s after initiating CM injection and has a temporal window of approximately 8–10 s. Therefore, to obtain a proper LAP by means of bolus tracking technique, a diagnostic delay of approximately 20 s should be selected (Laghi 2007; Foley 2002).

Hypervascular liver lesions, either benign or malignant, receive nearly all their blood supply from prominent neovasculature arising from the hepatic artery. Thus, they are best demonstrated during the LAP, in which they receive all their functional blood flow through the hepatic artery, virtually without any dilution from the unenhanced portal vein flow, enhancing to a greater degree than liver parenchyma (Foley 2002). Additionally, in clinical scenarios of portal hypertension, such as in liver cirrhosis, portal venous inflow is reduced, further increasing hypervascular lesion conspicuity during LAP images.

Right after the arterial circulation, the contrast-enhanced blood flows through the spleen, gut, and mesentery until it opacifies the portal vein. A dataset acquired at this time point is defined *portal venous phase (PVP)* and yields the maximal liver parenchymal enhancement. PVP occurs 60–80 s after initiating CM injection and is the most widely used acquisition phase in routine abdominal imaging, both in general-purpose abdominal CT scans and in oncologic settings (Foley 2002).

An adequate PVP shows homogeneous liver enhancement with a conspicuous opacification of hepatic veins and portal vein, which appear hyperdense compared to liver parenchyma (Federle and Blachar 2001). Such phase maximizes the detectability of hypovascular lesions, due to the combination of minimal arterial hepatic flow supplying these lesions and the significant enhancement of liver parenchyma (Soyer et al. 2004). On the contrary, hypervascular liver lesions may not be detectable on PVP since they enhance to the same degree of surrounding parenchyma.

Delayed phase (DP) occurs subsequently to PVP, begins 100–120 s after CM injection, and is characterized by gradual CM distribution in the hepatic interstitial spaces. Consequently, attenuation differences between focal liver lesions and liver parenchyma are minimized (Federle and Blachar 2001). Main indications for performing a DP are the investigation of hepatocellular carcinoma (Furlan et al. 2011), cholangiocarcinoma, and detection of liver metastases (Kanematsu et al. 2006). In clinical routine it is also useful to characterize cavernous hemangiomas, identified by the typical centripetal enhancement pattern (Kim et al. 2001). Figure 1 provides an overview of the different phases routinely acquired in liver imaging.

More delayed CT image set may be additionally acquired 10–15 min after CM injection only with specific indications, generally including suspected cholangiocarcinoma, primary sclerosing cholangitis, or any focal hepatic mass associated with intrahepatic bile duct obstruction: in such cases, in fact, it has been established that the presence of a large component of fibrosis causes a very characteristic prolonged stromal enhancement (Federle and Blachar 2001).

6 CT Perfusion

CT liver perfusion (CTP) is a promising functional imaging technique that aims to provide information about regional and global liver microcirculation and to improve the evaluation of hepatic parenchyma through the possibility of an early characterization of focal liver lesions (Meijerink et al. 2008). Perfusion imaging quantifies the transport of blood to a unit volume of tissue, per unit of time, through dynamic CT acquisitions, by repeatedly scanning the liver multiple times at short time intervals, during and after CM injection.

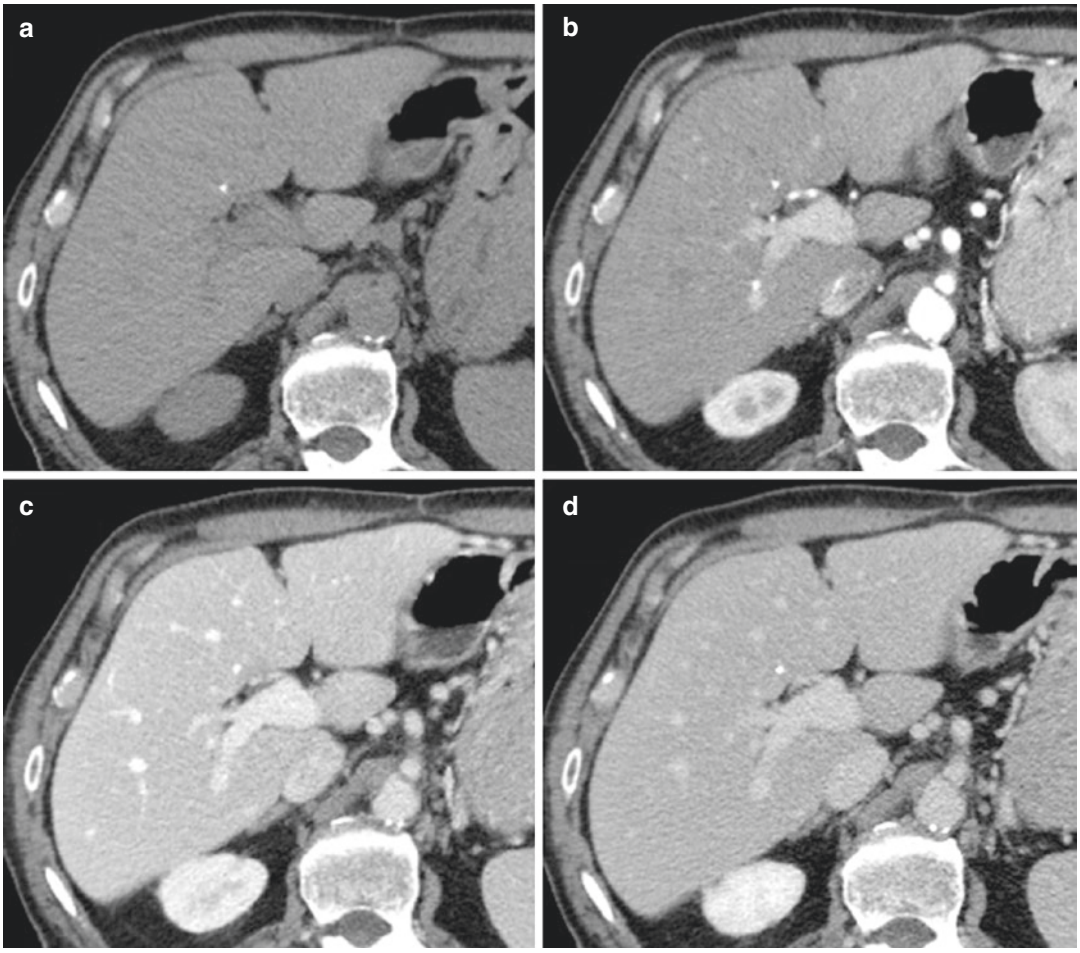

Fig. 1 Multiphasic liver CT examination. (**a**) Unenhanced phase demonstrates slightly higher parenchymal density than the portal venous system. A microcalcification is also easily identifiable. During late hepatic arterial phase (**b**) the aorta and the hepatic artery are the vessel characterized by the highest attenuation values, while portal vein and liver parenchyma enhance to a lesser degree. Subsequent portal venous phase (**c**) maximizes portal vein attenuation and liver enhancement, while the hepatic artery density is reduced. During delayed phase (**d**) the contrast medium is distributed in the hepatic interstitial spaces, and thus the attenuation differences between vessels and liver parenchyma are reduced

The basic principle of CTP is based on tissue attenuation changes, expressed in HU, which are directly proportional to the local concentration of CM within the tissue's microvasculature and interstitial space, as a function of time: the increase and subsequent decrease of CM concentration provide quantitative information about blood flow characteristics and allow quantification of the tissue vascularity (Sahani 2012).

Conventional CT can only achieve a qualitative assessment of contrast enhancement, since any time point during arterial, portal, and delayed phases represents a mixed result of entering and exiting of CM; CTP overcomes such limitations by allowing quantitative measurements (Kartalis et al. 2017).

The proper CTP protocol consists of a pre-contrast image acquisition, required to identify the optimal scan coverage, followed by dynamic sequential CT scanning of same volume, over time, after intravenous injection of CM (Kambadakone and Sahani 2009). The sequential dynamic image acquisition is necessary to obtain a time-attenuation curve (TAC), corresponding to

the arterial input function, which enables the evaluation of blood flow and its possible alterations. The TAC of the tissue being analyzed is compared to the time-intensity curve of a ROI placed into the lumen of the vessel supplying the tissue of interest. Because of dual circulatory liver dynamic, two different ROIs should be placed in the portal vein and in the abdominal aorta, respectively. This particular approach allows the estimation of both intravascular and extravascular properties. A single-input model assuming only a unique vascular supply has been proposed; however, it has not been validated because the separation of arterial and portal blood supply is an important information for characterization of focal lesions, enabling an early detection of alterations in liver perfusion (Kim et al. 2014).

After CM injection, it is possible to identify two different phases: *perfusion phase* and *interstitial phase* (Kartalis et al. 2017; Kambadakone and Sahani 2009):

- Perfusion phase (also called first-pass phase) is an intravascular phase study during which iodine is largely contained within the lumen of the vessels. It lasts approximately 40–60 s and it is mainly determined by the blood flow.
- Interstitial phase (also called second-pass phase or delayed phase) is an extravascular phase during which iodine passes into the extravascular-extracellular compartment. It lasts approximately 2–10 m and it is mostly influenced by CM passive diffusion, largely depending on the blood volume and the permeability of the capillaries to CM.

To achieve precise time-intensity curves CT scans are acquired without any table feed, during a scan time of 55 s with a gantry rotation time of 0.5 s. During first-pass phase one image/s is obtained, whereas a lower temporal resolution can be applied during the second-pass phase, allowing one image every 10 s (Sahani 2012).

A small volume of high-concentrated CM (30–60 mL followed by a 50 mL saline flush) has to be injected at >4–5 mL/s to obtain a short and sharp bolus. A tube voltage of 80–100 kVp with a tube current of 50–120 mAs may be employed to perform CTP, in order to maximize iodine conspicuity. A 5 mm image reconstruction thickness is usually suggested (Kim et al. 2014).

To avoid errors in the calculation of perfusion values, it is important to prevent beam-hardening artifacts performing CTP in areas without any metallic device and try to reduce motion and respiratory artifacts giving proper instruction to the patient regarding breath-holding.

CTP-acquired sets of images may be evaluated with three different methods (Kartalis et al. 2017):

1. Qualitative analysis, based on visual evaluation of TAC shape, morphology, and color-coded perfusion maps
2. Semiquantitative analysis, based on measurement of TAC peak enhancement times and peak attenuation values
3. Quantitative analysis, based on the application of kinetic models

Only the latter method allows the calculation of various perfusion parameters in the tissues being analyzed and it is, therefore, the more precise and recommended.

CTP quantitative analysis includes three different methods of study, which may be used for quantification of tissue perfusion and/or permeability (Sahani 2012; Kim et al. 2014):

- *Model-free maximum slope method*: Both hepatic arterial and portal perfusion are calculated (in mL/min/100 mL) using the time to peak splenic enhancement, which is considered as a time point indicating the end of arterial phase and the beginning of the portal venous phase of liver perfusion and, thus, used to separate HAP from PVP.

This method is very often used for the quantification of liver perfusion parameters, although it takes into consideration only the first-pass phase of the liver TAC. It assumes that there is no venous outflow (to achieve a condition of no venous outflow a very high injection rate of 15–20 mL/s should be employed, which is not

technically feasible in routine clinical practice) (Kim et al. 2014) and parameters such as blood volume, mean transit time (MTT), or capillary permeability surface product may not be calculated.

- *Compartment model-based method:* This analytical method is subdivided into two different mathematical modeling, usually indicated as "single compartment" and "dual compartment," respectively. The *single compartmental model* considers CM as confined in only one compartment, represented by both intravascular and extravascular spaces, freely communicating through sinusoid fenestrae. It is based on Fick's principles and estimates perfusion parameters from the maximal slope or from the peak height of the liver time-intensity curve normalized to the arterial input function. Parameters calculated by this analytical methods are (1) blood flow (BF, expressed as mL/min/100 mL) indicating volume flow rate of blood through liver vasculature; (2) blood volume (BV, expressed in units of mL/100 mL) representing the volume of blood flowing in the vasculature; and (3) MTT, indicating the average time it takes the blood to pass from the arterial to the venous flow.

The *dual (or two)-compartment model* assumes that CM is distributed between vascular and interstitial space considered as two separated compartments, allowing the evaluation of capillary permeability and the estimation of second-pass phase-related parameters, such as permeability surface area product (PSAP) and flow extraction product (FEP). PSAP is the result of permeability per total surface area of capillary endothelium in a unit mass of tissue (measured as mL/min/100 mL), whereas FEP is the result of blood flow per extraction fraction (EF, measured as mL/min/100 mL), with the latter representing the amount of CM passing in the extravascular space in a single passage through the vasculature.

- *Distributed parameter model-based method:* This analytical method assumes that there is a concentration gradient from the arterial inlet and the venous outlet at capillary level and a backward flux from the extravascular-extracellular compartment to the intravascular compartment. The parameters calculated by using a distributed model-based method are blood flow, blood volume, MTT, and permeability.

Even a combination of all these methods may be used.

Through the analysis of these quantitative parameters, functional information reflecting blood flow status is captured: because many liver diseases may affect the dual blood supply in a predictable way, CTP can be useful for diagnosis, risk stratification, and therapeutic monitoring of many pathologic processes (Fig. 2).

Allowing an estimation of angiogenesis, CTP may provide information regarding differential diagnosis between benign and malignant lesions: increased hepatic arterial blood flow and decreased portal venous flow, frequently observed in cirrhosis and liver tumors, both primary and metastatic, may be easily assessed (Ippolito et al. 2012; Guyennon et al. 2010).

CTP may also allow the prediction of prognosis based on tumor vascularity, reflecting tumor neoangiogenesis, that is known to be related to tumor aggressiveness (Garcia-Figueiras et al. 2013). Additionally, it may predict early response to oncologic therapy and monitor patients during treatment, especially assessing tumor response to antiangiogenic therapy which often induces disease stabilization, rather than changing tumor size, detectable by CTP much earlier than conventional morphologic imaging (Jiang et al. 2013).

Promising results have been accomplished also using CTP for early identification of tumor recurrence and for assessment of vascular layout after interventional procedures (Weidekamm et al. 2005; Choi et al. 2010).

Recent technical advances are addressing CTP's major limitations of high radiation exposure and motion artifacts, mainly by implementing low-tube-voltage techniques, iterative reconstruction algorithms, and motion correction tools of image registration software (Ng et al. 2011).

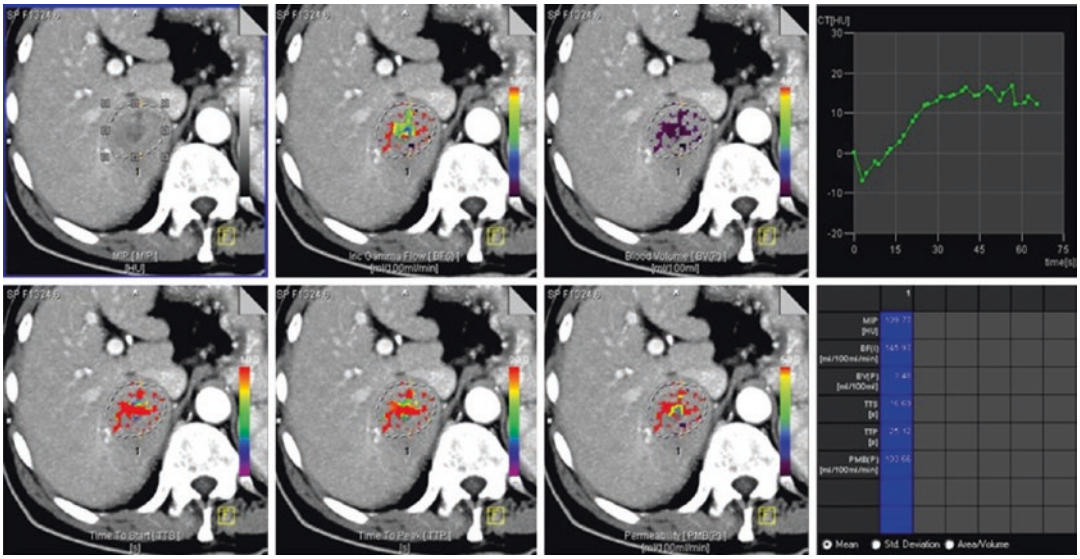

Fig. 2 Liver CT perfusion of a hepatocellular carcinoma. A region of interest is placed within the liver lesion and different parameters (blood flow, blood volume, time to start, time to peak, and permeability) are visually displayed on color-coded maps and precisely quantified (lower right). Time-attenuation curve (upper right) is eventually generated to depict variations of perfusion parameter as function of time

CTP still presents some limitations such as limited accessibility to perfusion software and lack of standardization in methods. However, these still unsolved problems are being addressed in the last few years.

7 Image Reconstruction

Over the years, different reconstruction algorithms have been developed to determine voxel attenuation values from raw and projection data. To date, reconstruction algorithms may be divided into two major categories:

- *Analytical algorithms*, with filtered back projection (FBP) being the most representative
- *Iterative algorithms*, such as statistical based and model-based reconstruction

7.1 Filtered Back Projection

It has been the standard CT reconstruction method for many years, due to its computational stability and short reconstruction time. FBP is a simple analytic method which ensures an adequate image quality by transforming intensity values transmitted at the detector in attenuation values in the projection domain. The latter are then filtered, using different reconstruction algorithms termed "kernels," to exploit peculiar image characteristics. Each kernel, in fact, has its trade-off between spatial resolution and noise: depending on the specific clinical application, a sharper or a smoother kernel may be used to obtain images with higher spatial resolution and increased image noise (e.g., to evaluate lung parenchyma) or images with lower noise and reduced spatial resolution, as recommended for imaging the liver and other soft tissues. Eventually, filtered projection data are back projected in the image domain (Geyer et al. 2015).

Various FBP-type algorithms were developed for different generations of CT scanners; however, all these approaches are based on simplifications such as the pencil-beam geometry of the X-ray and the intensity measurement performer only on a point located at the detector cell center, which affect the robustness.

Additionally, image acquired in specific clinical scenarios (reduced tube output or CT imaging of obese patients) may be affected by consistent image noise, due to the small number of photons

reaching the detectors. The result is increased image noise and blooming artifacts, which interfere with structure delineation and impair detectability of low-contrast lesions (Geyer et al. 2015; Fleischmann and Boas 2011).

7.2 Iterative Reconstruction

Iterative reconstruction (IR) was firstly introduced in 1970 and was originally implemented as reconstruction method in first cross-sectional images. However, due to lack of computational power and large amount of data in CT imaging, it was not clinically applicable for routine examinations. Recently, the advances of computational power and the greater attention given to radiation exposure have driven the renaissance of IR approach and the development of a variety of specific algorithms (Willemink and Noel 2018).

IR algorithms rely on a multistep image processing. First, an initial image estimation is created from the projection data, and the second step consists of the generation a new simulated image via a forward projection. Subsequently, the two images are compared, and in case of discrepancy, the first image is updated, through cyclic iterations, according to preselected objective parameters inherent in the algorithm.

Iterations may take place in the projection domain, in the image domain, or in both spaces, and these corrections are repeated until only minimal differences between the two datasets are found. Eventually, the final image is generated, characterized by both noise and artifact reduction and improved contrast and spatial resolution. Although the precise mechanism of each reconstruction algorithm is vendor specific and proprietary, IR algorithms may be classified into statistical based IR and model-based IR, depending on the models underlying the algorithm employed during the reconstruction process (Patino et al. 2015). However, irrespective of the algorithm being used, all IR techniques enable artifact reduction and, moreover, radiation dose savings without an excessive increase of image noise, which represents the main limitation of FBP in achieving diagnostic examinations at low radiation exposure. When applied in clinical practice, IR ensures high image quality and consistent dose reduction compared with FBP, down to 75% in selected clinical scenarios (Fig. 3) (Geyer et al. 2015; Willemink et al. 2013).

IR techniques have demonstrated their benefits also in liver imaging by improving lesion conspicuity and reducing image noise (Marin et al. 2010; Lv et al. 2015; Yu et al. 2013). Additionally, achieving dose reductions without affecting image quality may result to be particularly useful also in hepatic perfusion imaging, which traditionally requires high radiation doses. One of the limitations affecting IR is the generation of "plastic" or "blotchy" datasets, due to image oversmoothing. To mitigate this effect, hybrid reconstruction algorithms, combining FBP and IR, have been developed (Geyer et al. 2015).

In the last few years the scientific community has been working on applying artificial intelligence (AI) to improve CT images' reconstruction process, mostly employing neural networks, aiming at further optimizing image quality and reducing both radiation exposure and reconstruction time. Even though AI is not yet available for clinical implementation, it is expected to play an important role in IR in the foreseeable future (Litjens et al. 2017; Wang and Summers 2012).

8 Post-processing Techniques

The term "post-processing" refers to a specific procedure which enables to display CT images with characteristics—such as orientation and/or thickness viewing—different from those shown in the original presentation. Most common post-processing techniques include:

- Multiplanar reformatting (MPR)
- Maximum intensity projection (MIP)
- Minimum intensity projection (MinIP)
- Volume rendering (VR)

Each of these tools yields different insights into patients' anatomy and shows its peculiar strengths and limitations which impact clinical applications.

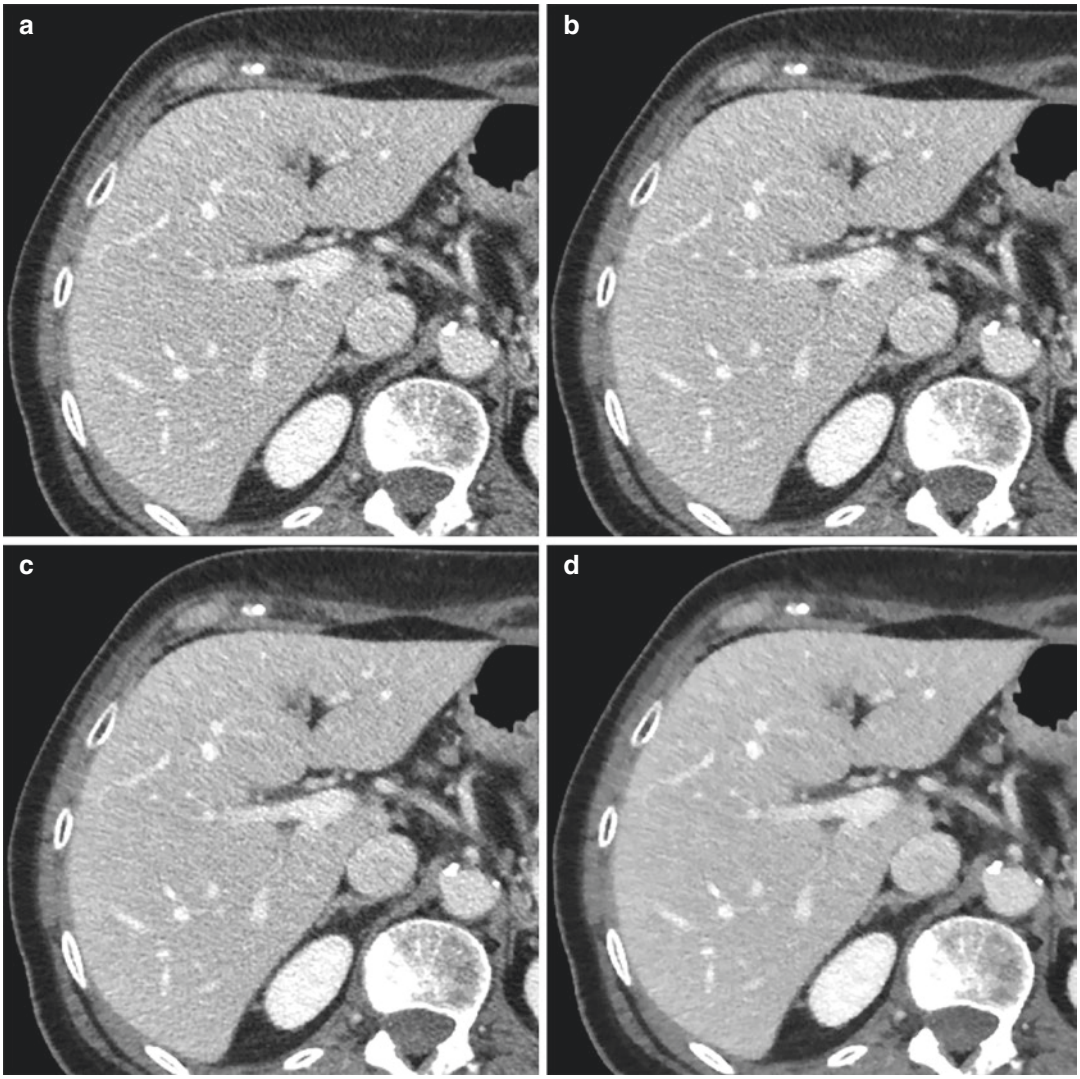

Fig. 3 (**a**) Shows a CT image reconstructed using filtered back-projection algorithm. Modern iterative reconstruction algorithms can be applied with low strength (**b**), medium strength (**c**), or high strength (**d**). Increasing levels of strength indicate a greater noise removal. The choice of the appropriate strength level depends on the clinical purpose and the optimal trade-off between dose reduction and image quality improvement. Despite less noisy, high strength levels (**d**) may result in "plastic" appearance

8.1 Multiplanar Reformatting (MPR)

It refers to planar cross sections oriented through planes other than the axial one, such as coronal and sagittal ones (Fig. 4). For non-orthogonal structures being imaged, oblique planes can also be derived. MPR utility in liver imaging has been especially established in lesion detection in difficult locations, such as subcapsular ones, and/or in heterogeneous parenchyma, such as occurs in cirrhotic liver. MPRs are also useful in the assessment of lesion-enhancing patterns and in the evaluation of tumor vascularity, for either vascular displacement, encasement, invasion, or

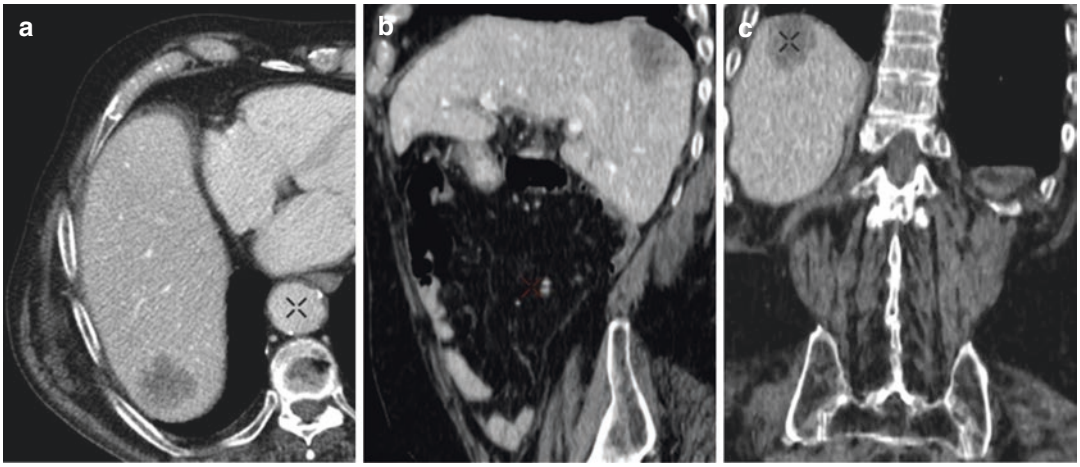

Fig. 4 Multiplanar reformatting images of the liver. Axial image (**a**) shows a hypovascular liver lesion located in the VII segment. Sagittal (**b**) and coronal (**c**) reformats allow for a more precise anatomical assessment especially in cases of subcapsular lesions

neoangiogenesis. Additionally, MPR reformatting may play an important role in preoperative planning, before hepatic surgery (Kamel et al. 2003).

8.2 Maximum Intensity Projection (MIP)

It employs parallel-viewing rays traced from the expected position of the operator and projected through the CT volume: only the highest density voxels detected along the ray path are depicted to be displayed along a predefined axis of the image, generating MIP images. MIP post-processing allows structures that are not in the same plane to be visualized along their entire length, such as occurs in hepatic arteries, providing also useful information about tumor vascularity, feeding vessels, and draining veins (Fig. 5). In general terms, MIP images are useful for depiction of vascular anatomy, providing CT angiography images useful in both preoperative planning of interventional procedures (i.e., chemoembolization) and postoperative evaluation of vascular complications (i.e., after liver transplantation), resulting as a valid tool also in focal lesion characterization due to increased conspicuity (Johnson and Fishman 2018).

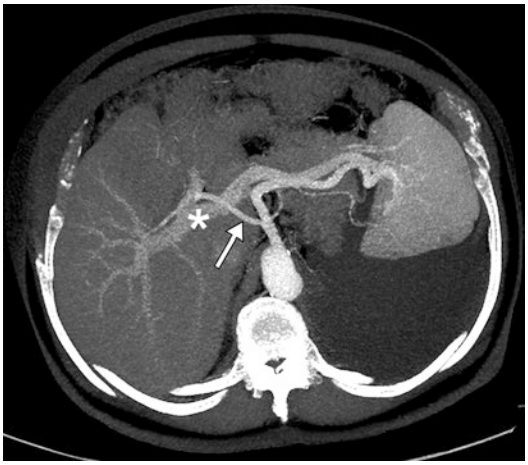

Fig. 5 Maximum intensity projection on the axial plane at the level of the hepatic hilum allows to depict on a single image the course of the hepatic artery (arrow) and the portal vein (asterisk) along with its intrahepatic branches

8.3 Minimum Intensity Projection (MinIP)

Conversely to MIP, only the lowest attenuation values detected along the ray path in each view are depicted to generate MinIP images. It is very useful in displaying structures with lower attenuation values such as the bile ducts and the hepatic biliary tree, showing more evident margins (Fig. 6) (Maher et al. 2004).

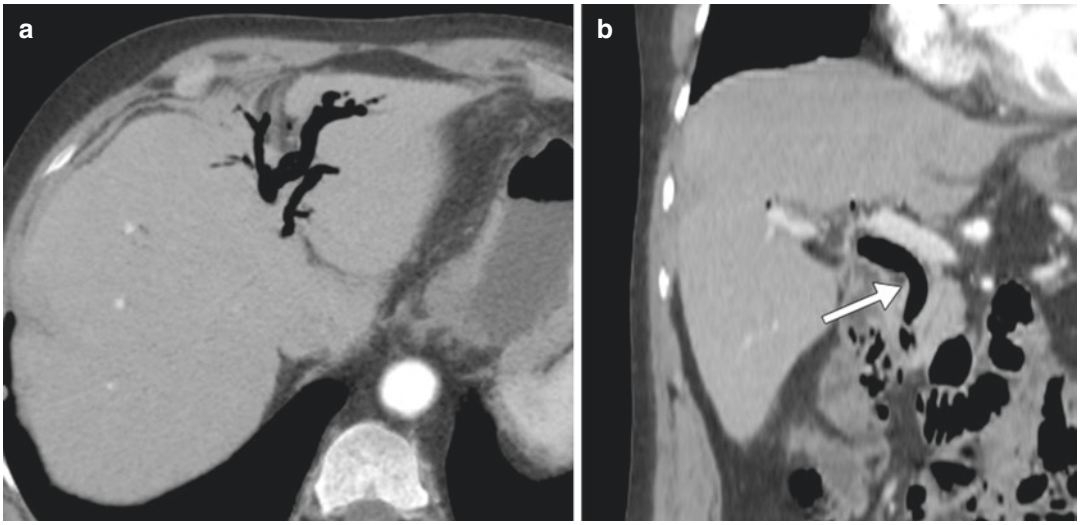

Fig. 6 Minimum intensity projection on the axial plane (**a**) and coronal plane (**b**) provides a comprehensive overview of the full extent of pneumobilia in a patient who had undergone endoscopic retrograde cholangiopancreatography. Pneumobilia involves the common bile duct and the intrahepatic ducts of liver segments II and IV

8.4 Volume Rendering (VR)

It produces 3D images, which can depict an entire organ or volume of interest in a single image. It consists of interpolating all data from scanned volume to provide realistic visualizations of objects, presented from multiple-view angles and freely rotating around an arbitrary point or plane of interest. All voxel values are assigned a color and an opacity level (from 0% to 100%) which may be interactively adjusted to alter the display in real time, possibly enhancing the visualization of particular structures within the imaged volume (Fig. 7) (Maher et al. 2004; Furlow 2014). VR enables the depiction of both hepatic arterial and venous anatomy with an optimal visualization of vascular details and potential anatomical variants, even better than angiography; moreover, it can provide a detailed overview of the liver architecture as well as orientation and characterization features of contingent masses. Moreover, VR reformatting may allow calculation of precise hepatic volumetry, which represents a clinical need in case of surgical planning for both liver transplantation and atypical resections, to evaluate remnant liver volume. Completely manual, semiautomatic, and completely automatic software are available to calculate liver volume, allowing a complete assessment in a single study, obviating other radiological procedures (Cai et al. 2016; Lodewick et al. 2016).

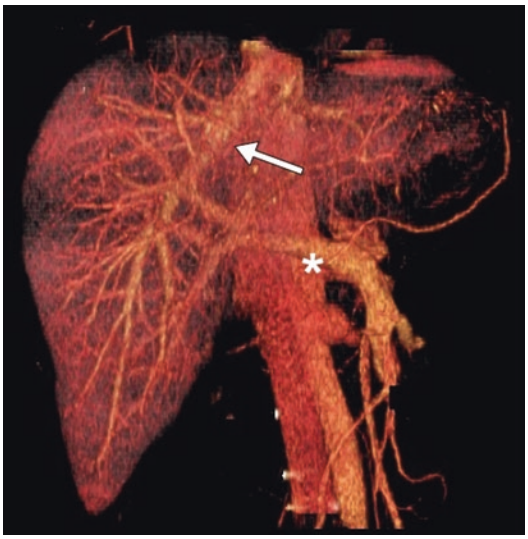

Fig. 7 Three-dimensional volume rendering of the liver on the axial plane provides a comprehensive overview of parenchyma and vessels, such as the portal vein (asterisk) and the hepatic veins (arrow)

Post-processing reformatting enables faster and more efficient interpretation of CT images and, with increasing computer processing power,

accuracy, specificity, and post-processing speed are expected to further improve.

9 Dual-Energy CT: Basic Principles and Technical Parameters

Dual-energy CT (DECT), also referred to as *spectral CT,* relies on a simultaneous acquisition of two datasets at different X-ray tube energy levels: a low-energy image dataset, acquired at 70–80 kVp, and a high-energy image dataset, typically acquired at 140–150 kVp. Various DECT techniques have been implemented, exploiting different methods to generate the two energy spectra:

- **Dual-Source DECT (dsDECT):** A single gantry is equipped with two independent X-ray tubes operating at two different potentials, with two corresponding opposite detector rows.
  Low-energy tube commonly operates at 80 kV, and high-energy tube operates at 140 kV. Depending on the scanner, other voltage settings such as 70, 90, and 100 kVp for low-energy tube and 150 kVp for high-energy tube are possible, especially in second- and third-generation dsDECT scanners (Siegel et al. 2016; McCollough et al. 2015; Flohr et al. 2006; Johnson et al. 2007). Disadvantages of such technology are the smaller field of view of the high energy, which may reduce the capability of evaluation of peripherally located abdominal structures in larger patients and the possibility of reduced material decomposition accuracy in rapidly moving structures (Forghani et al. 2017a).
- **Rapid-switching DECT (rsDECT):** The gantry is equipped with a single X-ray tube, performing multiple rapid alternations between high kVp and low kVp during a single gantry rotation. Such technology has a shorter temporal offset compared to dsDECT, leading to reduced beam-hardening artifacts and improved material decomposition accuracy. However, to adapt the two scan acquisitions at each position, rsDECT gantry rotation time is slower than in dsDECT, which might result in higher motion artifacts and nullify the short temporal offset (Furlow 2015).
- **Dual-layer detector DECT (dlDECT):** A combination of a single X-ray source, operating at a single tube potential, and a "sandwich" detector. The innermost layer of the detector is composed by a yttrium-based scintillator absorbing low-energy photons selectively, whereas the outermost detector consists of $Gd_2O_2S_2$ and absorbs high-energy photons (Siegel et al. 2016; McCollough et al. 2015). Spectral separation is limited because it occurs at the level of the detectors. Additionally, this design does not permit alterations of the spectra at the source. However, it ensures excellent temporal and spatial registration. More disadvantages are related to cross-scatter photons: low-energy photons may hit the outermost layer and vice versa, resulting in a contamination of datasets between the two detector layers (Forghani et al. 2017a).
- **Twin-beam DECT:** A combination of a single source and a single detector in which a split filter, consisting of gold, capable to decrease X-ray photon energy, and tin, capable to increase X-ray photon energy, is applied right after the X-ray source to obtain spectral separation. The resultant X-ray beam is split along the z-axis in a low-energy half and a high-energy half (Forghani et al. 2017a; Goo and Goo 2017).
  Advantages of this design include full FOV, relative hardware ease, and lower cost.
  Among the disadvantages, the need of a helical scan, to avoid a different portion of the patient being irradiated by the low- and high-energy spectra, must be considered. Additionally, the central part of the beam is composed by a mixed energy spectrum, disabling material discrimination from that portion of the data. Eventually, cross-scatter photons from one side of the beam may contaminate data at the other side of the beam (Forghani et al. 2017a).
- **Sequential DECT:** Two spiral or sequential scans are sequentially acquired at two different X-ray beams. This DECT design was the first one ever experimented, and may be performed in both volume and helical modes. In volume

mode, consecutive scans of the anatomic section are obtained using two single-rotation acquisitions, performed with different milliamperage settings for each kVp; however, this method was significantly affected by long interscan delay. The helical mode consists of consecutive scans of the entire volume obtained switching the tube potential at each anatomic section level (McCollough et al. 2015). The time delay between the two scans is relatively long and the temporal skew between the acquisitions is a significant disadvantage which may impair temporal registration, especially in moving organs or during contrast opacification. Furthermore, spectral data may be significantly distorted by any patient motion between the different acquisitions (Siegel et al. 2016; Forghani et al. 2017a).

10 Dual-Energy CT: Post-processing

10.1 Blended Images

Typically, the two image datasets acquired at high and low energy levels are by default blended together to generate images resembling conventional 120 kVp CT datasets, which radiologists are familiar with in clinical practice (Forghani et al. 2017b).

Blended images may be derived from linear blending algorithms with different proportion of low- and high-energy data in order to exploit different material characteristics: shifting blending ratio toward lower energies results in images with increased iodine signal but noisier, whereas moving blending ratio toward higher energies results in less image noise, as well as reduced iodine attenuation (Fig. 8) (Scholtz et al. 2015; Tawfik et al. 2012; Yu et al. 2012). Nonlinear blending algorithms may selectively combine information from both datasets with different weighting factors, improving contrast resolution and tissue characterization (Bongers et al. 2016).

10.2 Basis Material Decomposition

My means of basis material decomposition (BMD) the chemical composition of different materials is obtained by quantifying the X-ray attenuation measured at different X-ray energies.

SECT can differentiate tissues only on the basis of their attenuation coefficient (HU). However, HU shows consistent overlap between tissues and materials characterized by very different chemical composition. On the contrary, DECT uses the unique linear attenuation coefficients (μ) obtained by imaging at two different energies, and by modeling the energy

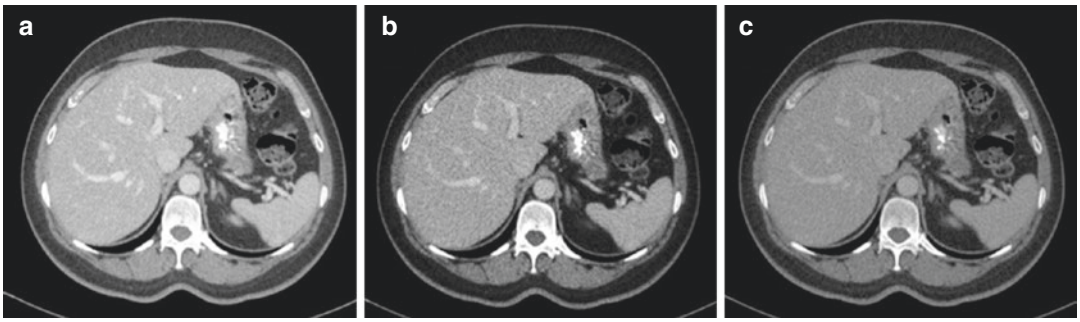

Fig. 8 Blended images generated by third-generation dual-energy dual-source CT scanner. Data from low-kVp tube and high-kVp tube are merged together to generate datasets resembling conventional 120 kVp images radiologist are accustomed to. (**a**) Depicts an image generated by a linear mixing of 90% data from low-kVp tube and 10% data from high-kVp tube. (**b**) Was generated by a blend of 60% data from low-kVp tube and 40% data from high-kVp tube, while (**c**) derives blending 30% data from low-kVp tube and 70% data from high-kVp tube. The higher the contribution of low-kVp tube data in the genesis of the image, the higher the image contrast and beam-hardening effect. The blending ratio can be freely modified by the operator based on the specific diagnostic task. Image courtesy of Dr. Moritz H. Albrecht—University Hospital Frankfurt

dependence of the photon on material mass density (ρ) and atomic number (Z), material-specific information may be obtained, providing diagnostic capabilities far beyond conventional CT (Silva et al. 2011; Marin et al. 2014).

Two different approaches are used, depending on the employed DECT technology:

- *Two-material decomposition*, used in single-source DECT
- *Three-material decomposition*, used in dual-source DECT

The first approach uses a specific algorithm applied in the projection space domain, before images are reconstructed from the low- and high-energy datasets: two selected materials having different atomic numbers and mass attenuation coefficients, most commonly including water and iodine, are used to obtain two sets of images. Consequently, all human tissues are expressed as function of the chosen basis pair. The second approach uses a different algorithm applied in the image space domain, after imaging reconstruction, and is based on the decomposition of three primary elements, generally iodine, soft tissue, and fat (Siegel et al. 2016). Precisely identifying iodine-containing pixels allows to generate a selective iodine material density display and subtract them from enhanced image, generating a virtual unenhanced display which corresponds to water material density image (Silva et al. 2011). Material decomposition can also be used in liver imaging to assess liver fat quantification (Hyodo et al. 2017).

10.3 Iodine Maps

Material decomposition allows quantifying the iodine content of a single pixel, expressed as mg/mL, with the consequent generation of selective images, representing iodine content in tissues. Such iodine-specific DECT datasets are named *iodine maps* and consist of images generated by assigning a color to the voxels containing iodine. They can be overlaid to standard grayscale images, allowing both qualitative assessment of iodine presence and quantitative measurement of the amount of iodine within a region of interest (Fig. 9) (Foley et al. 2016). Quantitative assessments and selective visualization of iodine CM permit to improve the conspicuity of iodine uptake and, thus, of lesion characterization (Siegel et al. 2016; Krauss 2018; Muenzel et al. 2017a).

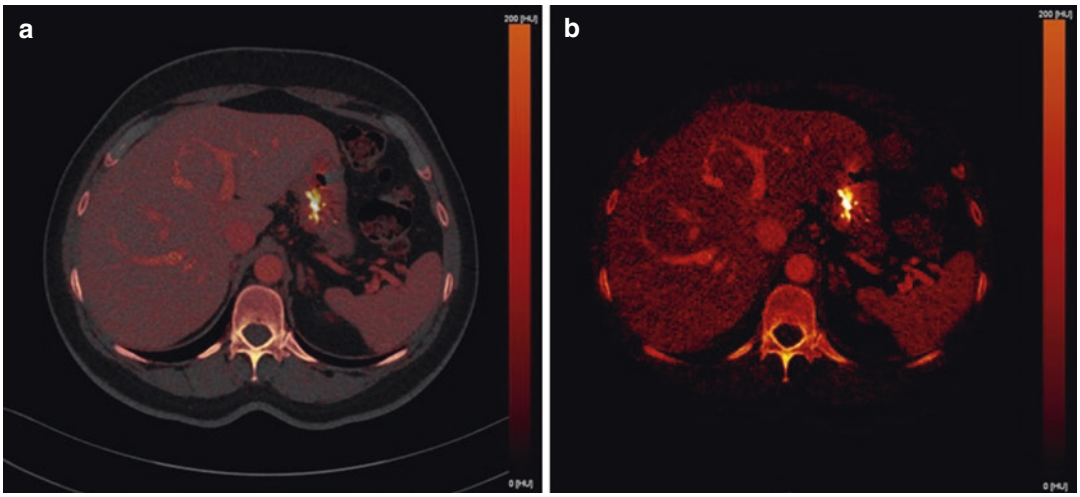

Fig. 9 Iodine map encodes the iodine distribution in each CT voxel and can be superimposed onto conventional CT dataset, with different percentages, resulting in a color-coded iodine overlay image (**a**: 50% superimposition; **b**: 100% superimposition). Red pixels reflect the presence of iodine, while the intensity of the color correlates with the amount of iodine. Image courtesy of Dr. Moritz H. Albrecht—University Hospital Frankfurt

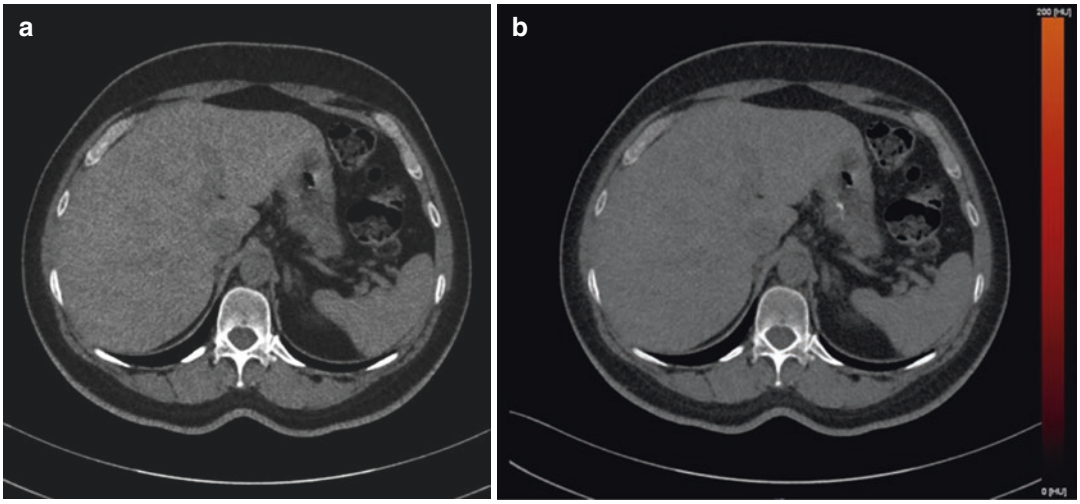

Fig. 10 Virtual non-contrast image (**a**) has comparable image quality of corresponding true non-contrast dataset (**b**), potentially allowing for a significant radiation dose saving by avoiding the need of a pre-contrast scan. Image courtesy of Dr. Moritz H. Albrecht—University Hospital Frankfurt

10.4 Virtual Non-contrast Images

The precise quantification of iodine distribution allows also the virtual removal of the iodine component from the CT number in each image voxel, produced by subtracting the iodine map from the enhanced DECT image (Kartalis et al. 2017; Goo and Goo 2017). The resultant virtual non-contrast (VNC) images have nowadays comparable image quality to true unenhanced datasets (Fig. 10). They allow substantial radiation dose and scanning time reduction by replacing true unenhanced images (Sauter et al. 2018). However, when assessing liver lesions after transarterial chemoembolization with lipiodol as a drug delivery system, true unenhanced images may be required for diagnostic purposes, since VNC alone might erroneously suggest enhancement and presence of viable tumor (Flemming et al. 2016).

10.5 Virtual Monoenergetic Images

X-ray beam used in conventional single-energy CT is polyenergetic, meaning it is composed by a broad spectrum of photons at different energy levels. DECT allows to generate virtual monoenergetic images (VMIs), which are particularly useful in reducing beam-hardening artifacts and increasing iodine attenuation.

VMIs are created in the projection domain or in the image domain, depending on the DECT technology (Yu et al. 2012). Low-keV VMIs, approximating the iodine K-edge (33.2 keV), are characterized by high contrast resolution. On the other hand, they are also intrinsically noisy. Conversely, high-keV VMIs are characterized by less image noise and reduced beam-hardening artifacts; nevertheless, they have low contrast resolution. It has been demonstrated that 60–75 keV VMIs may be considered equivalent to conventional 120 kVp SECT (Siegel et al. 2016) (Fig. 11).

Additionally, VMI may improve tissue characterization through the evaluation of the "spectral attenuation curves" generated by graphically plotting the attenuation values of a material as a function of energy, for every monochromatic energy of the spectrum. For example, iodine is known to show an attenuation peak at lower energies: only structures significantly enhancing after CM administration demonstrate sharp, sloping curves at lower kiloelectron-volt values, whereas structures not showing consistent CM

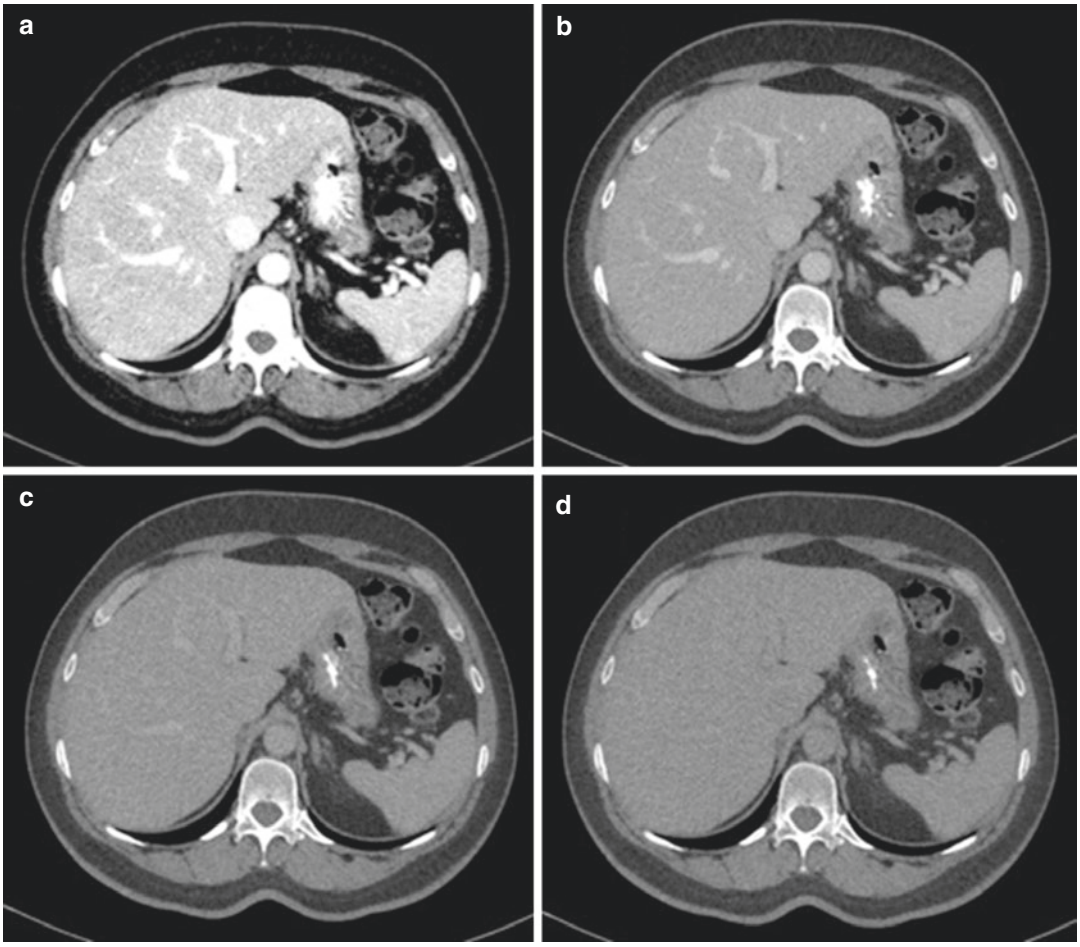

Fig. 11 Virtual monoenergetic images generated at (**a**) 40 keV, (**b**) 70 keV, (**c**) 100 keV, and (**d**) 130 keV. Low-keV monoenergetic images maximize iodine attenuation but are affected by relatively high image noise. Conversely, high-keV monoenergetic images are characterized by lower vascular contrast but reduce calcium blooming and beam-hardening artifacts. Image courtesy of Dr. Moritz H. Albrecht—University Hospital Frankfurt

enhancement display a relatively flatter kiloelectron-volt curve (Agrawal et al. 2014).

11 Future Perspective: Photon-Counting CT

CT scanners currently used in clinical practice are equipped with energy-integrating detectors. Such detector technology operates with a two-step process: the first step consists of absorbing the X-rays and converting them in visible light, which in turn is converted into electric signal by a photodiode. The amplitude of the electric signal is proportional to the total amount of energy that reaches the detectors.

Conversely, photon-counting detectors directly convert X-ray photons in electric signal, without the need of generating visible light. The height of the electrical pulses generated by each photon is proportional to the individual photon energy. The number of pulses exceeding a certain energy (set as threshold) contributes to the genesis of the image, while pulses below the energy threshold are considered as electronic noise and hence excluded from photon counts. Main advantages over photon-counting detectors over energy-integrating detectors are noise

reduction and consequent increased signal-to-noise ratio and increased spatial resolution.

More importantly, photon-counting detectors also differentiate multiple contrast agents (such as gadolinium and iodine); such characteristics might result in a single-acquisition multiphasic examination by injecting multiple contrast media at specific time points and then scanning the patient just once, reconstructing arterial and portal venous phase in post-processing. The implementation of this technology would be beneficial in terms of radiation dose savings and small lesion characterization, due to the perfect anatomic match of the different reconstructed phases. Photon-counting CT scanners (Muenzel et al. 2017b; Willemink et al. 2018) for humans are currently available only for research use. Manufacturers and researchers are actively working to optimize such CT systems and implement photon-counting CT in clinical practice in the foreseeable future.

References

Ad-Hoc Working Group of E, et al (2012) A European Renal Best Practice (ERBP) position statement on the Kidney Disease Improving Global Outcomes (KDIGO) clinical practice guidelines on acute kidney injury: part 1: definitions, conservative management and contrast-induced nephropathy. Nephrol Dial Transplant 27(12):4263–4272

Agrawal MD et al (2014) Oncologic applications of dual-energy CT in the abdomen. Radiographics 34(3):589–612

Awai K et al (2002) Aortic and hepatic enhancement and tumor-to-liver contrast: analysis of the effect of different concentrations of contrast material at multidetector row helical CT. Radiology 224(3):757–763

Bae KT (2010) Intravenous contrast medium administration and scan timing at CT: considerations and approaches. Radiology 256(1):32–61

Barrett JF, Keat N (2004) Artifacts in CT: recognition and avoidance. Radiographics 24(6):1679–1691

Boer P (1984) Estimated lean body mass as an index for normalization of body fluid volumes in humans. Am J Phys 247(4 Pt 2):F632–F636

Bongers MN et al (2016) Frequency selective non-linear blending to improve image quality in liver CT. RöFo 188(12):1163–1168

Bruce RJ et al (2009) Background fluctuation of kidney function versus contrast-induced nephrotoxicity. AJR Am J Roentgenol 192(3):711–718

Cai W et al (2016) Comparison of liver volumetry on contrast-enhanced CT images: one semiautomatic and two automatic approaches. J Appl Clin Med Phys 17(6):118–127

Caruso D et al (2018) Lean body weight-tailored iodinated contrast injection in obese patient: Boer versus James formula. Biomed Res Int 2018:8521893

Casillas VJ et al (2000) Imaging of nontraumatic hemorrhagic hepatic lesions. Radiographics 20(2): 367–378

Choi SH et al (2010) The role of perfusion CT as a follow-up modality after transcatheter arterial chemoembolization: an experimental study in a rabbit model. Investig Radiol 45(7):427–436

Federle MP, Blachar A (2001) CT evaluation of the liver: principles and techniques. Semin Liver Dis 21(2):135–145

Fleischmann D, Boas FE (2011) Computed tomography--old ideas and new technology. Eur Radiol 21(3):510–517

Flemming BP, De Cecco CN, Hardie AD (2016) Limitation of virtual noncontrast images in evaluation of a liver lesion status post-transarterial chemoembolization. J Comput Assist Tomogr 40(4):557–559

Flohr TG et al (2006) First performance evaluation of a dual-source CT (DSCT) system. Eur Radiol 16(2):256–268

Foley WD (2002) Special focus session: multidetector CT: abdominal visceral imaging. Radiographics 22(3):701–719

Foley WD et al (2016) White Paper of the Society of Computed Body Tomography and Magnetic Resonance on Dual-Energy CT, Part 2: Radiation Dose and Iodine Sensitivity. J Comput Assist Tomogr 40(6):846–850

Forghani R, De Man B, Gupta R (2017a) Dual-energy computed tomography: physical principles, approaches to scanning, usage, and implementation: part 1. Neuroimaging Clin N Am 27(3):371–384

Forghani R, De Man B, Gupta R (2017b) Dual-energy computed tomography: physical principles, approaches to scanning, usage, and implementation: part 2. Neuroimaging Clin N Am 27(3):385–400

Furlan A et al (2011) Hepatocellular carcinoma in cirrhotic patients at multidetector CT: hepatic venous phase versus delayed phase for the detection of tumour washout. Br J Radiol 84(1001):403–412

Furlow B (2014) CT image visualization: a conceptual introduction. Radiol Technol 86(2):187CT–204CT; quiz 205CT–207CT

Furlow B (2015) Dual-energy computed tomography. Radiol Technol 86(3):301ct–321ct; quiz322ct–325ct

Garcia-Figueiras R et al (2013) CT perfusion in oncologic imaging: a useful tool? AJR Am J Roentgenol 200(1):8–19

Geyer LL et al (2015) State of the art: iterative CT reconstruction techniques. Radiology 276(2):339–357

Goo HW, Goo JM (2017) Dual-energy CT: new horizon in medical imaging. Korean J Radiol 18(4): 555–569

Guyennon A et al (2010) Perfusion characterization of liver metastases from endocrine tumors: computed tomography perfusion. World J Radiol 2(11):449–454
Heiken JP et al (1995) Dynamic incremental CT: effect of volume and concentration of contrast material and patient weight on hepatic enhancement. Radiology 195(2):353–357
Hu H et al (2000) Four multidetector-row helical CT: image quality and volume coverage speed. Radiology 215(1):55–62
Hyodo T et al (2017) Multimaterial decomposition algorithm for the quantification of liver fat content by using fast-kilovolt-peak switching dual-energy CT: clinical evaluation. Radiology 283(1):108–118
Ippolito D et al (2012) Quantitative assessment of tumour associated neovascularisation in patients with liver cirrhosis and hepatocellular carcinoma: role of dynamic-CT perfusion imaging. Eur Radiol 22(4):803–811
James WPT, Waterlow JC, DHSS/MRC Group on Obesity Research (1976) Research on obesity: a report of the DHSS/MRC group, vol ix. H.M.S.O., London, p 94
Jiang T, Zhu AX, Sahani DV (2013) Established and novel imaging biomarkers for assessing response to therapy in hepatocellular carcinoma. J Hepatol 58(1):169–177
Johnson PT, Fishman EK (2013) Routine use of precontrast and delayed acquisitions in abdominal CT: time for change. Abdom Imaging 38(2):215–223
Johnson PT, Fishman EK (2018) Enhancing Image Quality in the Era of Radiation Dose Reduction: Postprocessing Techniques for Body CT. J Am Coll Radiol 15(3 Pt A):486–488
Johnson TR et al (2007) Material differentiation by dual energy CT: initial experience. Eur Radiol 17(6):1510–1517
Kambadakone AR, Sahani DV (2009) Body perfusion CT: technique, clinical applications, and advances. Radiol Clin N Am 47(1):161–178
Kamel IR, Georgiades C, Fishman EK (2003) Incremental value of advanced image processing of multislice computed tomography data in the evaluation of hypervascular liver lesions. J Comput Assist Tomogr 27(4):652–656
Kanbay M et al (2017) Serum uric acid and risk for acute kidney injury following contrast. Angiology 68(2):132–144
Kanematsu M et al (2006) Imaging liver metastases: review and update. Eur J Radiol 58(2):217–228
Kartalis N, Brehmer K, Loizou L (2017) Multi-detector CT: liver protocol and recent developments. Eur J Radiol 97:101–109
Kim T et al (2001) Discrimination of small hepatic hemangiomas from hypervascular malignant tumors smaller than 3 cm with three-phase helical CT. Radiology 219(3):699–706
Kim SH, Kamaya A, Willmann JK (2014) CT perfusion of the liver: principles and applications in oncology. Radiology 272(2):322–344
Kondo H et al (2010) Body size indexes for optimizing iodine dose for aortic and hepatic enhancement at multidetector CT: comparison of total body weight, lean body weight, and blood volume. Radiology 254(1):163–169
Krauss B (2018) Dual-energy computed tomography: technology and challenges. Radiol Clin N Am 56(4):497–506
Kwasa EA, Vinayak S, Armstrong R (2014) The role of inflammation in contrast-induced nephropathy. Br J Radiol 87(1041):20130738
Laghi A (2007) Multidetector CT (64 slices) of the liver: examination techniques. Eur Radiol 17(3):675–683
Lee CH et al (2013) Use of positive oral contrast agents in abdominopelvic computed tomography for blunt abdominal injury: meta-analysis and systematic review. Eur Radiol 23(9):2513–2521
Lee CH et al (2016) Water as neutral oral contrast agent in abdominopelvic CT: comparing effectiveness with Gastrografin in the same patient. Med J Malaysia 71(6):322–327
Litjens G et al (2017) A survey on deep learning in medical image analysis. Med Image Anal 42:60–88
Lodewick TM et al (2016) Fast and accurate liver volumetry prior to hepatectomy. HPB (Oxford) 18(9):764–772
Lv P et al (2015) Combined use of automatic tube voltage selection and current modulation with iterative reconstruction for CT evaluation of small Hypervascular hepatocellular carcinomas: effect on lesion conspicuity and image quality. Korean J Radiol 16(3):531–540
Maher MM et al (2004) Techniques, clinical applications and limitations of 3D reconstruction in CT of the abdomen. Korean J Radiol 5(1):55–67
Marin D et al (2010) Low-tube-voltage, high-tube-current multidetector abdominal CT: improved image quality and decreased radiation dose with adaptive statistical iterative reconstruction algorithm--initial clinical experience. Radiology 254(1):145–153
Marin D et al (2014) State of the art: dual-energy CT of the abdomen. Radiology 271(2):327–342
McCollough CH et al (2015) Dual- and multi-energy CT: principles, technical approaches, and clinical applications. Radiology 276(3):637–653
Meijerink MR et al (2008) Total-liver-volume perfusion CT using 3-D image fusion to improve detection and characterization of liver metastases. Eur Radiol 18(10):2345–2354
Moos SI et al (2013) Contrast induced nephropathy in patients undergoing intravenous (IV) contrast enhanced computed tomography (CECT) and the relationship with risk factors: a meta-analysis. Eur J Radiol 82(9):e387–e399
Muenzel D et al (2017a) Material density iodine images in dual-energy CT: detection and characterization of hypervascular liver lesions compared to magnetic resonance imaging. Eur J Radiol 95:300–306
Muenzel D et al (2017b) Simultaneous dual-contrast multi-phase liver imaging using spectral photon-counting computed tomography: a proof-of-concept study. Eur Radiol Exp 1(1):25
Ng CS et al (2011) Reproducibility of CT perfusion parameters in liver tumors and normal liver. Radiology 260(3):762–770

Patino M et al (2015) Iterative reconstruction techniques in abdominopelvic CT: technical concepts and clinical implementation. AJR Am J Roentgenol 205(1):W19–W31

Patnana M et al (2018) Liver calcifications and calcified liver masses: pattern recognition approach on CT. AJR Am J Roentgenol 211(1):76–86

Pickhardt PJ et al (2012) Specificity of unenhanced CT for non-invasive diagnosis of hepatic steatosis: implications for the investigation of the natural history of incidental steatosis. Eur Radiol 22(5):1075–1082

Sahani D (2012) Perfusion CT: an overview of technique and clinical applications. http://cds.ismrm.org/protected/10MProceedings/files/Tues%20E09_02%Sahani.pdf

Sauter AP et al (2018) Dual-layer spectral computed tomography: virtual non-contrast in comparison to true non-contrast images. Eur J Radiol 104:108–114

Scholtz JE et al (2015) Non-linear image blending improves visualization of head and neck primary squamous cell carcinoma compared to linear blending in dual-energy CT. Clin Radiol 70(2):168–175

Siegel MJ et al (2016) White Paper of the Society of Computed Body Tomography and Magnetic Resonance on Dual-Energy CT, Part 1: Technology and Terminology. J Comput Assist Tomogr 40(6):841–845

Silva AC et al (2011) Dual-energy (spectral) CT: applications in abdominal imaging. Radiographics 31(4):1031–1046. discussion 1047-50

Soyer P et al (2004) Detection of hypovascular hepatic metastases at triple-phase helical CT: sensitivity of phases and comparison with surgical and histopathologic findings. Radiology 231(2):413–420

Spearman JV et al (2016) Effect of automated attenuation-based tube voltage selection on radiation dose at CT: an observational study on a global scale. Radiology 279(1):167–174

Stacul F et al (2011) Contrast induced nephropathy: updated ESUR contrast media safety committee guidelines. Eur Radiol 21(12):2527–2541

Tawfik AM et al (2012) Dual-energy CT of head and neck cancer: average weighting of low- and high-voltage acquisitions to improve lesion delineation and image quality-initial clinical experience. Investig Radiol 47(5):306–311

Thomas ME et al (2015) The definition of acute kidney injury and its use in practice. Kidney Int 87(1):62–73

van der Molen AJ et al (2018a) Post-contrast acute kidney injury—part 1: definition, clinical features, incidence, role of contrast medium and risk factors: recommendations for updated ESUR contrast medium safety committee guidelines. Eur Radiol 28(7):2845–2855

van der Molen AJ et al (2018b) Post-contrast acute kidney injury. Part 2: risk stratification, role of hydration and other prophylactic measures, patients taking metformin and chronic dialysis patients: recommendations for updated ESUR contrast medium safety committee guidelines. Eur Radiol 28(7):2856–2869

Wang S, Summers RM (2012) Machine learning and radiology. Med Image Anal 16(5):933–951

Weidekamm C et al (2005) Effects of TIPS on liver perfusion measured by dynamic CT. AJR Am J Roentgenol 184(2):505–510

Willemink MJ, Noel PB (2018) The evolution of image reconstruction for CT-from filtered back projection to artificial intelligence. Eur Radiol

Willemink MJ et al (2013) Iterative reconstruction techniques for computed tomography part 2: initial results in dose reduction and image quality. Eur Radiol 23(6):1632–1642

Willemink MJ et al (2018) Photon-counting CT: technical principles and clinical prospects. Radiology 289(2):293–312

Williamson EE, McKinney JM (2001) Assessing the adequacy of peripherally inserted central catheters for power injection of intravenous contrast agents for CT. J Comput Assist Tomogr 25(6):932–937

Yu L, Leng S, McCollough CH (2012) Dual-energy CT-based monochromatic imaging. AJR Am J Roentgenol 199(5 Suppl):S9–S15

Yu MH et al (2013) Low tube voltage intermediate tube current liver MDCT: sinogram-affirmed iterative reconstruction algorithm for detection of hypervascular hepatocellular carcinoma. AJR Am J Roentgenol 201(1):23–32